Multiscale damage in co-cured composites - Perspectives from experiments and modelling

Subramanian, N.; Bisagni, C.

Publication date
2021

Document Version
Final published version

Published in
36th Technical Conference of the American Society for Composites 2021

Citation (APA)
Subramanian, N., & Bisagni, C. (2021). Multiscale damage in co-cured composites - Perspectives from experiments and modelling. In O. Ochoa (Ed.), *36th Technical Conference of the American Society for Composites 2021: Composites Ingenuity Taking on Challenges in Environment-Energy-Economy, ASC 2021* (pp. 1479-1492). (36th Technical Conference of the American Society for Composites 2021: Composites Ingenuity Taking on Challenges in Environment-Energy-Economy, ASC 2021; Vol. 3).

Multiscale Damage in Co-Cured Composites—Perspectives from Experiments and Modelling

NITHYA SUBRAMANIAN and CHIARA BISAGNI

SUMMARY

Bonded and co-cured composites are popular alternatives to structures joined with mechanical fasteners in aircraft but the complex and coupled damage mechanisms in the co-cured/bonded region are poorly understood, thus making the evaluation of their strength and durability difficult with current modelling strategies. This study explores the potential of interleaf inclusion in failure-prone, critical regions of co-cured composite specimens in improving the joint strength and interface fracture toughness and strives to advance the understanding of damage initiation in the co-cured region using an atomistic model.

A two-pronged approach is pursued here with bench-scale experimental testing and molecular modelling in this study. Experiments are performed for mode I fracture toughness with double cantilever beam (DCB) on composite laminates with an epoxy interleaf layer. Two epoxy resins and three methods for interleaf inclusion are explored in this study; we supplement the results from DCB testing with insights from confocal microscopy on the crack tip and the interleaf layer pre- and post-testing. Molecular dynamic (MD) simulations capture the cohesive interactions at the three-phase interface containing the carbon fiber, the prepreg epoxy, and the interleaf epoxy. Results highlight that an interleaf layer made from partially-cured and filmed epoxy, further consolidated in the composite lay-up is the most effective way to suppress void formation, improve dispersion, and maximize cohesive interactions at the interface of co-cured composites.

Nithya Subramanian, Marie Sklodowska-Curie Postdoctoral Fellow, Faculty of Aerospace Engineering, Delft University of Technology, Delft, Zuid Holland, The Netherlands
Chiara Bisagni, Professor, Faculty of Aerospace Engineering, Delft University of Technology, Delft, Zuid Holland, The Netherlands

INTRODUCTION

Thermoset epoxies are ubiquitous in fiber reinforced composites as matrix materials. They enable effective load transfer, particularly in the transverse direction of continuous fiber composites that are widely used as light-weight structural materials in automotive, aerospace, and other multifunctional applications. However, thermoset epoxies are brittle [1–3] and the mechanisms of damage initiation (polymer crazing or bond scission causing void formation [4]) in them are difficult to predict, thus limiting their applications. The interfacial interactions between the matrix and the fiber also critically determine the composite's resistance to interlaminar stresses that eventually lead to crack formation and growth. Thus, the interlaminar fracture toughness is a parameter of key interest to the design, manufacturing, and analyses communities to assess the performance of composites under quasi-static, fatigue, and impact loading conditions. Testing for the interlaminar fracture toughness is performed through protocols [5] that allow the estimation of the energy required to initiate and propagate a crack under mode I, mode II, and/or mixed mode loading conditions.

Interleaved composites or composite laminates with an interleaf layer where a discrete layer of epoxy (thermoset or thermoplastic) is inserted between adjacent plies have been studied in the past [6–8] as a strategy to improve mode I and II fracture toughness. Recent studies have also investigated the effectiveness of short fibers [9], soft materials [10], thin films [11,12], nanofiber membranes/mats [13] as interleaf materials resulting in varying degrees of success. Extra resin film layers made of the same or a compatible resin, embedded among the reinforcing fibers have improved both mode I and mode II fracture toughness in numerous studies [14,15]. The investigation of a same resin interleaf by Singh et al. [16] showed an increase of 70% for mode I, and 200% for mode II fracture toughness by interleaving the carbon/epoxy prepreg with 50 μm and 200 μm thick layers. The fracture morphology of epoxy interleaved laminates under mode II loading revealed larger damage zones owing to micro-crack diffusion mechanisms than those of the reference composite materials. Furthermore, the chemical and mechanical linkages formed between the interleaf epoxy, the fiber, and the prepreg matrix form a three-phase interface and potentially create tortuous crack paths. Despite the scientific interest in interleaved composites, fundamental models that shed light on the interactions at this three-phase interface do not exist, to the best of our knowledge.

Interleaved epoxy layers can be consolidated in the composite laminate using various techniques. The quality of the interleaf layer is determined by dispersion of the epoxy, uniform thickness, and its ability to form chemical/mechanical linkages with the surrounding material phases. While the direct inclusion of uncured epoxy in the prepreg allows for maximized crosslink formation, the pressure required to consolidate the fibers in the prepreg is often too high and makes it challenging to control the thickness of an interleaf layer comprised of uncured epoxy. Studies in the past [17,18] have investigated the partial cure of epoxy systems – a process often referred to as 'B-staging' – and the incorporation of the partially-cured epoxy as a filmed layer in the composite. This grants the ability to control the mobility/flow (therefore, also the dispersion), thickness, and weight/volume fraction of the epoxy in the interleaved composite while also facilitating the formation of crosslink bonds in the secondary

cure stage. However, in order to design an effective partial (and a subsequent full cure) cycle for an epoxy system, its cure chemistry must be fully understood. Chemical-mechanical coupling plays a vital role in the behavior of polymers and their interaction with the fibers in the composite. This multiphysical coupling is important because of the chemical crosslink formation followed by the changes to rheology and phase transformation (causing cure shrinkage) in the thermoset during the cure process.

In this study, we investigated the link between the cure chemistry of a polymer and its effectiveness as an interleaf layer in a composite laminate. We performed bench-scale DCB tests that yielded information about the fracture toughness and the damage propagation in the interleaf layer. Molecular simulations shed light on the nature of physical and chemical interactions between the fiber, prepreg matrix and the interleaf polymer phases in the hybrid composite system. This research with a synergistic experimental and computational framework is expected to provide insight into the effectiveness of interleaf inclusions and the multiscale evolution of damage in hotspots and further help the design of co-cured joints in larger aerospace structures.

METHODOLOGY

Epoxy Filming

Two different epoxy resins were considered as candidates for the interleaf layer due to the similarity of their manufacturer-provided cure cycles and mechanical properties to that of the Hexcel 8552 system, which comprises the prepreg (IM7/8552) used in our composite laminates. The chosen epoxy systems in this study are both thermoset polymers referred to as Epilok 60-434 (Bitrez Co.) – a single component epoxy, and API-60 (Kaneka Aerospace Inc.) – a two-component with curing agent. The first step was to characterize their rheology and cure chemistry in order to effectively integrate them in co-cured composite laminates.

The filming of the thermoset polymer was performed in a high-temperature oven under atmospheric pressure based on the partial cure cycles designed from differential scanning calorimetry (DSC) data. The epoxy was mixed (in the case of API-60) and introduced between two Teflon films (250µ thickness) embedded between glass slabs. The glass slabs and the Teflon films were coated with liquid release agent in order to allow the peeling of the filmed epoxy. The thickness of the filmed layer was controlled by introducing metal strips of predefined height in between the Teflon layers. For Epilok 60-434, the filming cycle corresponded to an initial temperature ramp to 140°C at 3°C per minute followed by an isothermal cycle for 45 minutes. Subsequently, the oven was cooled down at 3°C per minute and the system was allowed to cool until the glass slabs reached room temperature (measured with a thermocouple). The filming cycle for API-60 was an initial temperature ramp to 105°C at 1°C per minute followed by an isothermal cycle for 45 minutes (cooled at 1°C per minute). Once the system was cooled to room temperature, the Teflon films containing the B-staged epoxy were removed from within the glass slabs; the required dimensions were cut out and each side of the Teflon film was peeled off to expose the filmed epoxy. Figure 1 shows the outcomes of the filming process for both epoxy systems. While a constant thickness

film with good dispersion and low void content was obtained in both cases, the Epilok 60-434 film was brittle and difficult to peel from the Teflon film while maintaining structural integrity. With the two-component API-60 polymer system, film thicknesses of 100µ and 250µ were created and embedded in the samples.

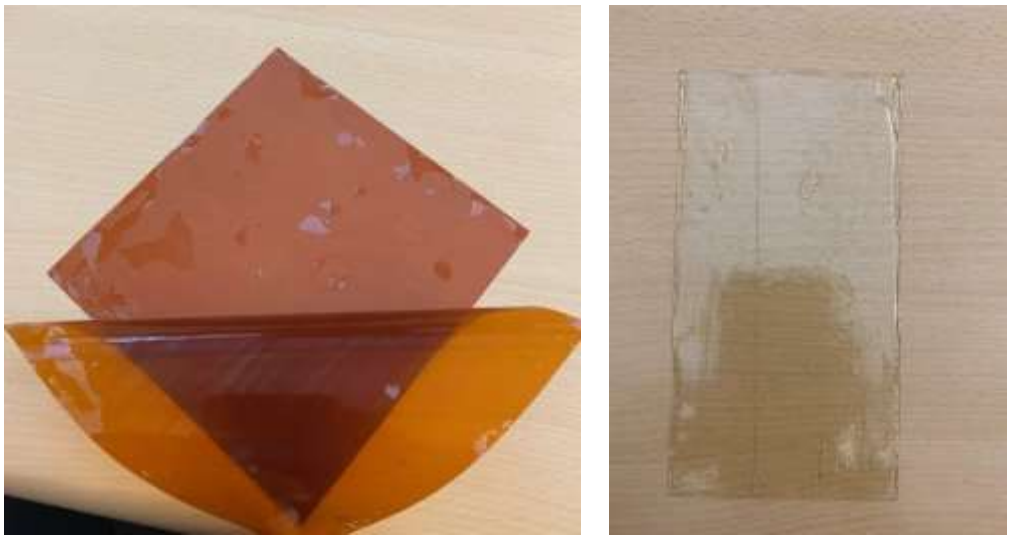

(a) (b)

Figure 1. B-staged epoxy films created from the two epoxy systems; (a) Epilok 60-434 filmed between Teflon sheets resulting in a brittle film that lost its structural integrity during the Teflon peeling; (b) API-60 filmed and peeled from Teflon sheets and cut to required dimensions. The edges are frayed from the peeling and subsequent handling process.

Interleaving and Consolidation

Embedding the epoxy interleaf layer into the composite laminate has been pursued in different ways in literature [9,14,16]. Two competing mechanisms at play need to be considered. The first is the ability of the interleaf polymer to form chemical bonds with itself and consolidate into physical adhesion with the prepreg epoxy and the fiber surfaces, thus potentially offering more resistance to crack growth. The second is to control the flow and mobility of the interleaf epoxy so it disperses uniformly and maintains a predefined thickness (and does not get ejected from the laminate during cure). The incorporation of uncured polymer in the interleaf improves the chances of the first mechanism whereas a filmed interleaf improves the possibility of the second mechanism.

In our study, we focused on three different techniques for interleaving: (i) introducing uncured epoxy in between cured half laminates; (ii) introducing filmed/B-staged epoxy in between cured half laminates; (iii) introducing filmed/B-staged epoxy in IM7/8552 prepreg stacks. For the first two cases, the half laminates were cured in the autoclave following the Hexcel cure cycle for monolithic composite parts. The secondary cure cycle varied based on manufacturer data (for the uncured epoxy) and our DSC data (for the filmed epoxy). The last technique entailed a single-step cure process where the filmed epoxy and the prepreg was cured all at once in the autoclave.

In this technique, the pressure in the autoclave was reduced to 4 Bar compared to the recommended cure pressure for the prepreg (7 Bar) in order to ensure that the filmed epoxy would maintain its film thickness during cure. Since the Epilok 60-434 could not be reliably filmed, the combination of the above three techniques yielded five types of samples. All the samples have the same ply layup: [0_{12}//interleaf//0_{12}]. The description of the samples including their physical dimensions, the way they were manufactured, and the type of interleaf they contain are provided in Table 1.

TABLE 1. SAMPLE TYPES AND DESCRIPTIONS.

Sample type	Description of laminate and interleaf
Sample 1	Cured half laminates with uncured Epilok 60-434 in the mid-plane
Sample 2	Cured half laminates with filmed Epilok 60-434 in the mid-plane
Sample 3	Cured half laminates with uncured API-60 in the mid-plane
Sample 4	Cured half laminates with filmed API-60 in the mid-plane
Sample 5	Prepreg consolidation with filmed API-60 in the mid-plane and single-step cure process

Mechanical Testing

Double cantilever beam tests were performed in accordance with the ASTM standards where the specimens were loaded with a piano hinge. The length and width of the DCB specimen are not relevant parameters for this standard test. However, the nominal dimensions of the samples were 150 × 25 × 3 mm. The initial delamination was created by embedding two layers of Teflon release films of 25μ thickness each. The specimens were bonded to loading blocks (20 × 25 × 6 mm). The initial embedded delamination in the specimens was 30 mm (measured from the edge of the specimen). The standard procedure recommends an initial loading and unloading step to pre-crack the DCB specimen and ensure a sharp singular crack-front. This step was executed, and the initial delamination lengths were nominally 40 mm, i.e., a_0 = 20 mm measured from the edge of the loading block.

The general test set up consisted of a 10kN Zwick tension/compression testing machine with a 1kN load cell. The data collection software testXpert III was employed to register the load-displacement data in combination with a webcam and an image acquisition toolkit to record images at fixed intervals. The test set up along with a zoomed-in image of a specimen with markings every 1 mm is shown in Figure 2. During the initial pre-cracking stage, a loading rate of 0.5 mm/minute was maintained and the crack tip was observed visually until a crack length of 30 mm (from the load line) was attained. Upon the completion of pre-cracking, a manual clicker was used to pause the load frame, acquire images for 5 seconds and subsequently, unload at 10 mm/min. During the reloading test stage, the loading rate was 0.5 mm/minute and images were acquired every 0.5 seconds during the test.

(a) (b)

Figure 2. (a) Test set up of the load frame and the aligned camera. (b) zoomed-in image of specimen during the reloading stage with markings to monitor the crack tip.

Molecular Modelling

The interphase region containing the interleaf serves as the propagating medium for the embedded crack in this study. Therefore, accurate modeling techniques are integral to study the effects of this complex region on the composite response. In composites infused with an epoxy interleaf, the interphase region is more complex due to the presence of multiple constituents and their interactions with each other that eventually dictate the toughness and strain energy release associated with the growth of cracks. An atomistic methodology to simulate the constituent interphases in carbon fiber epoxy interleaved composite is presented in this study as well. Experimental investigations at material interfaces are challenging due to the limitations in direct measurement techniques, test specimen size and preparation, and uncertainty in the data from indirect measurements. Computational methods using atomistic simulations have been used in literature to understand the physical and chemical parameters that affect the mechanical response of interphases in multiphase materials [19–21].

Molecular dynamics (MD) simulations have tremendously contributed to the study of physical and chemical interactions in multiphase materials. However, the high computational cost associated with the atomistic simulations limits their use beyond the nanoscale. Hence, the modeling of carbon/graphite fibers that have diameters in the order of microns is not feasible via MD simulations. In our previous work, the relevant section of the fiber (at the interface) was modeled using irregularly stacked graphene layers with induced voids [22]. The epoxy resin and hardener molecules penetrate these voids and form crosslink bonds in the presence of dispersed CNTs. Thus, the molecular model captures the physical entanglements formed by the polymer chains with graphene layers representing adhesion at the semi-crystalline fiber surface. Additionally, another polymer phase was introduced to the system to model the interleaf epoxy. The overall simulation volume is illustrated in Figure 3.

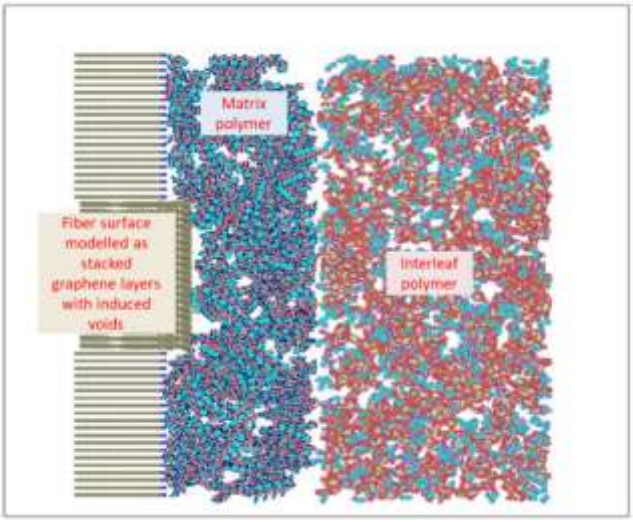

Figure 3. Molecular simulation volume containing the outer surface of the carbon fiber; this is modelled through layered graphene sheets with large voids where polymer chains can get entangled during the cure process. The matrix polymer and the interleaf polymer phases are also modelled explicitly.

The crosslinking process in the polymer was simulated using a cut-off distance-based bond formation approach. When the actives site of the resin and hardener chains are closer than a predefined cut-off distance (4.5 Å), a chemical bond is assigned to the site [23]. Interatomic interaction terms that represent the van der Waals and electrostatic forces are obtained from Merck molecular force field (MMFF) for the atoms in the polymer phases and the all-atom optimized potential for liquid simulations (OPLS-AA) for the atoms in the graphene layers. The pairwise Lennard-Jones energy was calculated using $E_{pair} = 4\epsilon\left[\left(\frac{\sigma}{r}\right)^{12} - \left(\frac{\sigma}{r}\right)^{6}\right]$ where r is the distance between two particles, and ϵ and σ are the maximum depth of the potential energy well and the distance of zero potential, respectively. Lennard-Jones interaction terms between dissimilar atom types are calculated via Lorentz–Berthelot mixing rules. We employ a cutoff distance of 10 Å for short-range interactions. The simulations are performed in LAMMPS [24] with non-periodic boundary conditions along the *x* axis. Subsequent to equilibration for and crosslinking simulations in the NPT ensemble (P = 1 atm, T = 298 K), the overall potential energies and the individual interaction energies between the phases are extracted.

RESULTS AND DISCUSSION

DCB Tests

The force-displacement curves for the unidirectional samples with different interleaving methods are shown in Figure 4. Each type of interleaved sample has two specimens manufactured from the same composite plate and subsequently cut to fit DCB standard dimensions. It is easily notable that Sample 5 manufactured with the single-step cure method has the highest crack initiation load and the slowest crack propagation rate. There is also good reproducibility of data between specimens that

belong to the same sample. The occurrence of multiple sudden load drops along the force-displacement curve indicates unstable crack propagation and this phenomenon is particularly dominant in Samples 1 and 2. While Sample 5 exhibits a rather smooth behavior, there are still two major load drops (in 5.1 for instance) corresponding to a rapid opening of the crack tip. One specimen from each sample was tested to complete failure (as seen by the final load drop to zero in Figure 4) and the other was unloaded after reaching about 75% of the failure displacement. A variability in the stiffness can be observed between the two specimens in Samples 1 and 4, as seen from the slopes of the initial linear region. This could be attributed to the differences in the dispersion and uniformity of the interleaf within the same Sample.

The ASTM testing procedure recommends noting the displacement and crack length at which the visual onset of delamination occurs. This visual onset point was easy to determine for Samples 1-4 and their load displacement curves also provide strong supporting data to determine this point with sharp initial load drops. Brittle matrices are known to have a unique point where the onset of delamination occurs (the first change from a_0) and where non-linearity begins in their load-displacement curve. Sample 5, on the other hand, exhibits a softer curve for the load drop and the visual onset of crack growth was more difficult to observe. The point of nonlinearity was ~3% off from the displacement at which crack growth was seen. This indicates that the interleaved epoxy at the crack front could be described as a tough matrix.

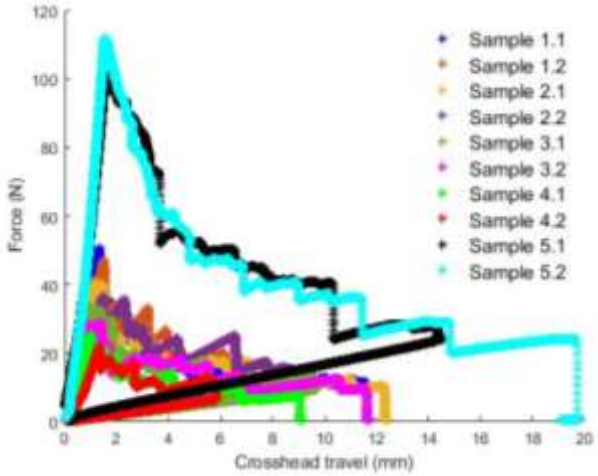

Figure 4. Load-displacement curves from DCB tests on the different interleaved epoxy composite samples.

The corresponding crack length information for the load-displacement data was inferred from the acquired images. A MATLAB code was written with the support of functions in the Image Processing toolbox. The acquired images were cropped, gray-scaled, binarized, and segmented to obtain the relevant sections and remove noise. Figures 5(a) and (b) show the cropped and the final segmented versions of a sample image. Firstly, a calibration index was determined for each set of images (from each test) to convert the number of pixels along a line to a corresponding length value in millimeters. Since the total length of the specimen was known in advance, we focused on constructing a bounding box for the pristine section of the specimen. The number

of pixels along the mid-line of the largest bounding box that encapsulates the pristine section (white pixels) was computed. This number was multiplied by the calibration index and then subtracted from the total length of the specimen to obtain the crack length at each instant. Note that this results in some outliers and discrepancies in output when there is large bending and rotation of the specimen.

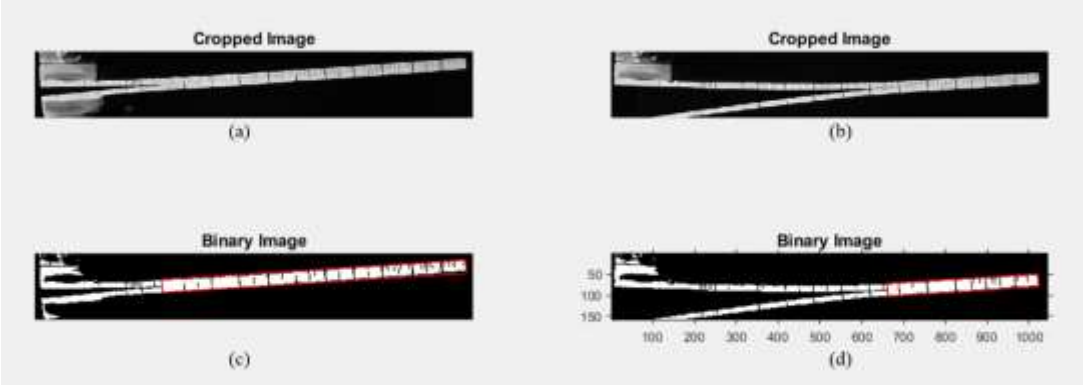

Figure 5. Image processing of acquired snapshots during the DCB tests. (a) and (b) cropped sections of images at two different time instants of the test; (c) and (d) are the binarized equivalents of the cropped images and show the largest bounding box encapsulating the uncracked/pristine section of the specimen at a given instant. The dimensions of this bounding box are used to compute the instantaneous crack lengths.

The calculated crack lengths are plotted against the crosshead displacement data from the test software in Figure 6. Based on the values of *a* at which sudden, unstable crack jumps occur, we were able to focus on specific critical regions for post-failure microscopy of the fracture surfaces (*see SI)*. In almost each case, poor interfacial adhesion was confirmed either owing to the presence of microscopic voids or non-uniformity in interleaf thickness (sudden change in thickness). In Samples 1 and 2, a clear multiphase interface between the prepreg epoxy and interleaf epoxy was also observed and the presence of interfacial asperities between these two polymer phases also led to the crack path being non-planar. Therefore, the estimation of fracture toughness of these two interleaf interfaces were significantly complicated because the assumption of planar, uniform, and unidirectional crack growth was no longer valid. Sample 5 exhibits a steady crack growth pattern barring one or two instances of crack jumps, which are attributed to the presence of voids at the crack tip that instant. Microscopic characterization of the pristine sample (Sample 5) shows the uniform dispersion and thickness of interleaf epoxy behind the initial crack tip allowing a homogeneous plastic zone and the steady growth of delamination.

From Figures 4 and 6, it can be deduced that the calculation of fracture toughness with the modified beam theory (MBT) is difficult for Sample 1 and 2. Therefore, the load data was smoothed with a noise filter and a window spanning 0.5% of the size of the data set in each case. Subsequently, the initiation mode I fracture toughness was calculated using the modified compliance calibration (MCC) method. This method was chosen for two reasons: (i) the statistics of the output property yielded the lowest coefficient of variation with this method; (ii) this method accounts for the thickness of the specimen. The thickness of Sample 5 was about 4.1mm whereas that of the other

samples was around 3.2 mm. This is because the autoclave pressure during cure was reduced to 4 Bar, and this resulted in lower compaction of the fibers.

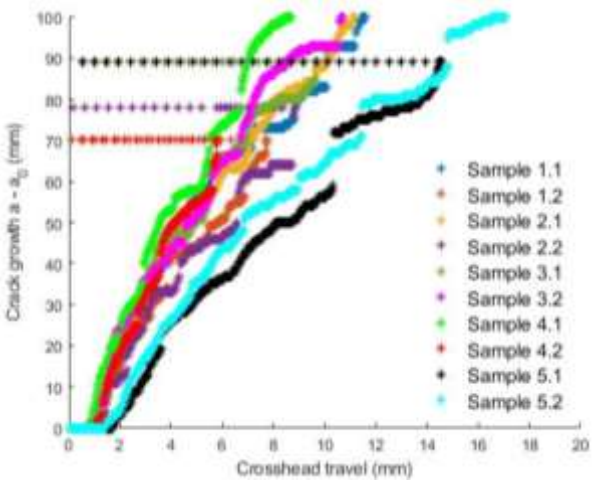

Figure 6. Crack growth vs. crosshead displacement.

$$G_I = \frac{3P^2C^{2/3}}{2A_1bh} \tag{1}$$

In Equation (1), *P* corresponds to the load, *b* and *h* are the width and thickness of the specimen, respectively. *C* is the compliance of the specimen deduced from the load-displacement data. A least squares plot of the crack length normalized by specimen thickness *(a/h)* is generated and plotted against the cube root of compliance ($C^{1/3}$). The slope of the linear fit for this plot yields the value of A_1. The calculated values of the initiation mode I fracture toughness for each specimen are listed in Table 2.

TABLE 2. INITIATION FRACTURE TOUGNESS IN MODE I.

Specimen/ Sample ID	G_{I_MCC} **(N/m)**
1.1	100.4
1.2	108.6
2.1	80.69
2.2	73.09
3.1	59.64
3.2	47.3
4.1	33.63
4.2	35.75
5.1	304.5
5.2	306.5

The load-displacement as well as the crack growth data make it abundantly clear that the method of interleaf consolidation exerts significant influence on damage propagation mechanisms. The choice of interleaf epoxy material is also critical to improving the fracture toughness of the laminate. An interleaved composite laminate made with Epilok 60-434 is tougher in mode I failure if incorporated as uncured resin as opposed to being filmed and subsequently interleaved. This could be attributed to the poor quality and brittle nature of Epilok film. Peeling the film and incorporating it in the mid-plane layer led to some chips and breaks that may have introduced discontinuities in the interleaf layer. The uncured Epilok resin with its low viscosity (50 mPas at 25°C) is able to flow and disperse well in the mid-plane layer. However, the curing process under pressure (2 Bar) led to the resin being pushed out of the laminate and resulting in a lower thickness than planned.

The API-60, on the other hand, offers poor resistance to crack growth in both uncured and filmed interleaf formats when forced into adhesion with cured half laminates. The mixture of the API-60 resin and the curing agent is highly viscous (60,000 cPas at 65°C) and the uncured mixture is difficult to spread evenly on the half laminates at room temperature. The filmed version on the other hand maintains its thickness and cohesion; however, since the film is already partially cured, the secondary cure process fails to generate any bond formation between the interleaf epoxy and the prepreg polymer resulting in the worst fracture resistance among all the samples that were investigated.

Thus, the best outcome is obtained by incorporating a filmed epoxy in the mid-plane of uncured prepreg stacks. The trade-off between the two competing mechanisms of interleaf thickness/dispersion uniformity as well as bond formation with the fiber and matrix is best accomplished in this manufacturing scenario. This is further confirmed by images from microscopy where the two polymer phases appear to be smooth and cohesive, hardly generating any phase contrast among them *(see SI)* in the case of Sample 5. The initiation fracture toughness of Sample 5 indicates a significant improvement compared to a composite laminate of equivalent thickness and ply lay-up with no interleaf. Data in literature for the initiation mode I fracture toughness for unidirectional $[0_{12}//0_{12}]$ laminates range between 200 and 280 N/m [25] and the inclusion of an epoxy interleaf yields a substantial increase to this value.

MD Simulations

Results from our MD simulations help unravel some of the physical and chemical interactions among the different phases in the composite system and explain the behavior of the samples during mechanical testing. Although the molecular simulations do not directly correlate with mode I fracture testing, the potential energies and the energy required to separate the phases apart provide interesting and relevant information to the parsing of test data. The aim of the molecular models is to investigate the individual interaction between phases; first we focus on the interaction between the fiber and the matrix polymer, then on the interaction between the matrix polymer and the interleaf polymer. Figure 7 shows the physical separation of the matrix polymer from the fiber surface. During this separation, the polymer chains entangled at the interface stretch first. As the chains start to break (first drop in pair

energy around 3% strain), an added resistance is offered by the entanglement between the polymer chains and the graphene sheet voids. Finally, a strain of 15% corresponds to the complete separation of the two phases. Allowing the polymer chains to cure in the presence of the fiber surface containing voids and imperfects creates better cohesion at the fiber/matrix interface.

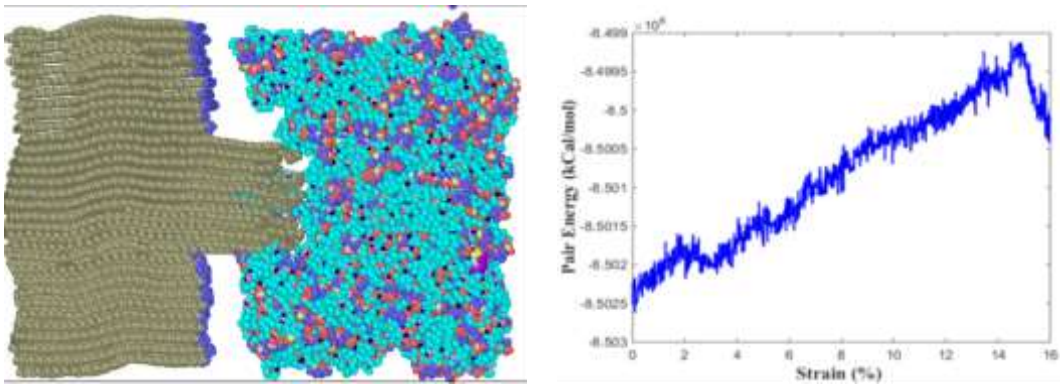

(a) (b)

Figure 7. Molecular simulation results of the fiber/matrix interface. (a) physical separation of the matrix polymer chains from the fiber surface showing entanglement of the chains with the fibroids; (b) correlated pair energy variation between the two phases during separation.

The second interface of interest is the one between the two polymer phases. This interface was investigated by means of two approaches. In the first approach, each polymer phase was separately cured (allowed to form crosslink bonds based on the cut-off distance-based method) and the simulation volume was constructed with already crosslinked polymer chains. In the second approach, uncured resin and hardener molecule chains of both polymers were introduced in a simulation volume in separate box regions. While they were initially equilibrated with a wall boundary in between, the crosslinking simulation was performed for 0.5 ns at NPT conditions with interactions allowed between the two phases. Chemical bond formation was restricted only to specific active sites (for e.g., the matrix resin could form chemical bonds only with the matrix hardener, and the interleaf resin could for chemical bonds only with the interleaf hardener molecule), but the equilibration allowed for chains of the two polymers to be physically entangled with each other. Therefore, although both cases only allow for physical interactions between the two polymer types, the second scenario creates physical chain entanglements because the two polymers are allowed to simultaneously undergo curing in the presence of each other. This accounts for the manufacturing scenario for Sample 5 where both the Hexcel 8552 matrix and the API-60 epoxy undergo chemical curing simultaneously while being physically compacted.

The results from these two molecular simulation approaches are presented in Figure 8. The first case shows a steady linear increase in the energetic interaction following by a sharp steep drop of the pair correlation energies. This confirms that the interfacial interactions steeply dissipate as the distance between the two polymer phases increases while being separated. On the other hand, the molecular system with chain entanglement between the two phases displays a more gradual degradation of the energetics. Multiple mechanisms are at play here offering resistance to the separation

of phases such as the extension of the individual chains themselves as well as the disentangling of chains belonging to different polymers. The higher values of pair energies indicate a stronger interaction between the polymer phases and this in turn, could offer more resistance to the propagation of micro-cracks as they propagate through this medium. Such an improved interaction would explain the drastically better performance of Sample 5 in the DCB tests as well.

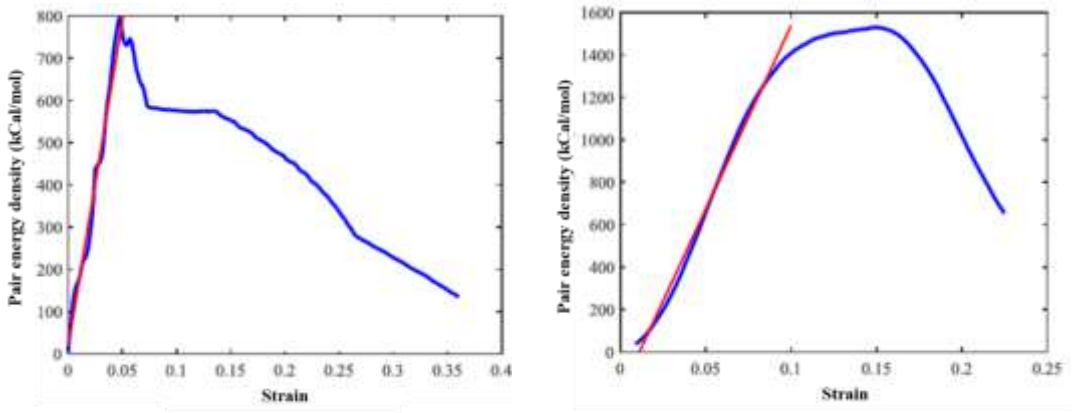

Figure 8. Molecular simulation results for the two-polymer interface (a) pair energies between polymer phases when crosslink simulations are performed independently and crosslinked chains introduced into simulation volume; (b) pair energies between polymer phases when crosslinking is allowed to happen simultaneously in the two polymer systems.

CONCLUSIONS

The inclusion of an interleaved epoxy layer in a composite laminate and its effect on mode I fracture toughness was investigated in this study. Multiple techniques were explored to consolidate the epoxy as interleaf in the laminate including the consideration of two different epoxy systems as candidates for interleaf and different means of their integration. We employed several tools at our disposal to investigate the cure chemistry of the epoxy systems and characterize their microstructure as interleaf materials in a 'neat' as well as filmed/B-staged form. Mode I DCB tests yielded valuable insights into the damage propagation mechanisms in the interleaf medium. Results from the mechanical tests showed that both chemical as well as physical interactions between the polymer phases need to be maximized to generate effect interleaved composites. The specimens that were manufactured while allowing both the prepreg epoxy and the interleaf epoxy to undergo chemical curing in the presence of each other offered the most resistance to crack growth; they also registered initiation fracture toughness values significantly higher than reference laminates of the same ply lay-up with no interleafs. The molecular simulations provided clarity to the nature of physical and chemical interactions among the multiple phases in this hybrid composite system. Simulations of the separation of phases from each other showed that the formation of polymer chain entanglements with each other as well as with the fiber surface improves the pair energetics and increases the overall forces required to cause delamination. This integrated study, combining bench-scale testing and nanoscale modelling furthers our understanding of damage growth in interleaved media and will help the design of composite joints with interleafs in the co-cured region.

REFERENCES

[1] Rottler J, Barsky S, Robbins MO. Cracks and Crazes: On Calculating the Macroscopic Fracture Energy of Glassy Polymers from Molecular Simulations. Phys Rev Lett 2002;89:148304.

[2] Naebe M, Abolhasani MM, Khayyam H, Amini A, Fox B. Crack Damage in Polymers and Composites: A Review. Polym Rev 2016;56:31–69.

[3] Awaja F, Zhang S, Tripathi M, Nikiforov A, Pugno N. Cracks, microcracks and fracture in polymer structures: Formation, detection, autonomic repair. Prog Mater Sci 2016;83:536–73.

[4] Karger-Kocsis J. Microstructural and molecular dependence of the work of fracture parameters in semicrystalline and amorphous polymer systems. Eur. Struct. Integr. Soc., vol. 27, Elsevier; 2000, p. 213–30.

[5] Johnson W, Masters J, O'Brien T, O'Brien T, Martin R. Round Robin Testing for Mode I Interlaminar Fracture Toughness of Composite Materials. J Compos Technol Res 1993;15:269.

[6] Tanimoto T. Interleaving methodology for property tailoring of CFRP laminates. Compos Interfaces 2002;9:25–39.

[7] Ozdil F, Carlsson LA. Mode I Interlaminar Fracture of Interleaved Graphite/Epoxy. J Compos Mater 1992;26:432–59.

[8] Chen SF, Jang BZ. Fracture behaviour of interleaved fiber-resin composites. Compos Sci Technol 1991;41:77–97.

[9] Zhou H, Du X, Liu H-Y, Zhou H, Zhang Y, Mai Y-W. Delamination toughening of carbon fiber/epoxy laminates by hierarchical carbon nanotube-short carbon fiber interleaves. Compos Sci Technol 2017;140:46–53.

[10] Meijer G, Ellyin F. Effect of a Soft Interleaf on Transverse Cracks in Thick Glass Fiber–Epoxy Cross-ply Laminates. J Compos Mater 2004;38:2199–211.

[11] Jiang W, Tjong SC, Chu PK, Li RKY, Kim JK, Mai YW. Interlaminar Fracture Properties of Carbon Fibre/Epoxy Matrix Composites Interleaved with Polyethylene Terephthalate (Pet) Films. Polym Polym Compos 2001;9:141–5.

[12] Yun NG, Won YG, Kim SC. Toughening of carbon fiber/epoxy composite by inserting polysulfone film to form morphology spectrum. Polymer 2004;45:6953–8.

[13] Palazzetti R, Zucchelli A, Gualandi C, Focarete ML, Donati L, Minak G, et al. Influence of electrospun Nylon 6,6 nanofibrous mats on the interlaminar properties of Gr–epoxy composite laminates. Compos Struct 2012;94:571–9.

[14] Marino SG, Czél G. Improving the performance of pseudo-ductile hybrid composites by film-interleaving. Compos Part Appl Sci Manuf 2021;142:106233.

[15] Shin YC, Lee WI, Kim HS. Mode II interlaminar fracture toughness of carbon nanotubes/epoxy film-interleaved carbon fiber composites. Compos Struct 2020;236:111808.

[16] Singh S, Partridge IK. Mixed-mode fracture in an interleaved carbon-fibre/epoxy composite. Compos Sci Technol 1995;55:319–27.

[17] Zheng N, Liu H-Y, Gao J, Mai Y-W. Synergetic improvement of interlaminar fracture energy in carbon fiber/epoxy composites with nylon nanofiber/polycaprolactone blend interleaves. Compos Part B Eng 2019;171:320–8.

[18] Reichanadter A, Bank D, Mansson JE. A novel rapid cure epoxy resin with internal mold release. Polym Eng Sci 2021;61:1819–28.

[19] Bhowmik R, Katti KS, Katti D. Molecular dynamics simulation of hydroxyapatite–polyacrylic acid interfaces. Polymer 2007;48:664–74.

[20] Subramanian N, Koo B, Venkatesan KR, Chattopadhyay A. Interface mechanics of carbon fibers with radially-grown carbon nanotubes. Carbon 2018;134:123–33.

[21] Subramanian N, Whittaker ML, Ophus C, Lammers LN. Structural Implications of Interfacial Hydrogen Bonding in Hydrated Wyoming-Montmorillonite Clay. J Phys Chem C 2020;124:8697–705.

[22] Subramanian N, Rai A, Chattopadhyay A. Atomistically derived cohesive behavior of interphases in carbon fiber reinforced CNT nanocomposites. Carbon 2017;117:55–64.

[23] Subramanian N, Rai A, Chattopadhyay A. Atomistically informed stochastic multiscale model to predict the behavior of carbon nanotube-enhanced nanocomposites. Carbon 2015;94:661–72..

[24] Plimpton S. Fast Parallel Algorithms for Short-Range Molecular Dynamics. J Comput Phys 1995;117:1–19.

[25] Raimondo A, Urcelay Oca I, Bisagni C. Influence of interface ply orientation on delamination growth in composite laminates. J Compos Mater 2021.